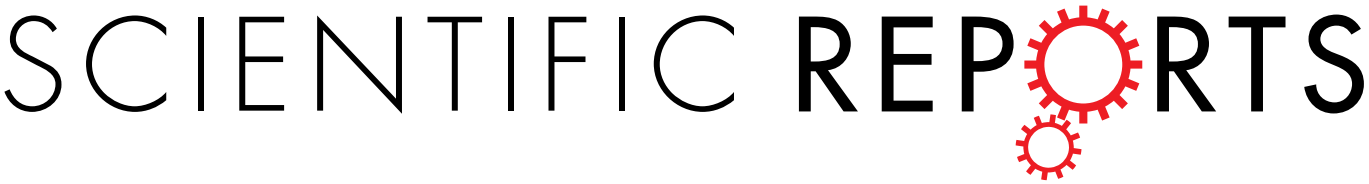

OPEN

A High Affinity Red Fluorescence and Colorimetric Probe for Amyloid β Aggregates

Received: 21 October 2015
Accepted: 07 March 2016
Published: 01 April 2016

K. Rajasekhar[1], Nagarjun Narayanaswamy[1], N. Arul Murugan[2], Guanglin Kuang[2], Hans Ågren[2] & T. Govindaraju[1]

A major challenge in the Alzheimer's disease (AD) is its timely diagnosis. Amyloid β (Aβ) aggregates have been proposed as the most viable biomarker for the diagnosis of AD. Here, we demonstrate hemicyanine-based benzothiazole-coumarin (TC) as a potential probe for the detection of highly toxic $Aβ_{42}$ aggregates through switch-on, enhanced (~30 fold) red fluorescence ($E_{max} = 654$ nm) and characteristic colorimetric (light red to purple) optical outputs. Interestingly, TC exhibits selectivity towards $Aβ_{42}$ fibrils compared to other abnormal protein aggregates. TC probe show nanomolar binding affinity ($K_a = 1.72 \times 10^7\ M^{-1}$) towards $Aβ_{42}$ aggregates and also displace ThT bound to $Aβ_{42}$ fibrils due to its high binding affinity. The $Aβ_{42}$ fibril-specific red-shift in the absorption spectra of TC responsible for the observed colorimetric optical output has been attributed to micro-environment change around the probe from hydrophilic-like to hydrophobic-like nature. The binding site, binding energy and changes in optical properties observed for TC upon interaction with $Aβ_{42}$ fibrils have been further validated by molecular docking and time dependent density functional theory studies.

The misfolding driven aggregation process of Aβ peptides in the brain is one of the main causes of Alzheimer's disease (AD)[1–3]. The neurodegeneration and subsequent progressive deterioration in cognitive ability are hallmark symptoms of this incurable syndrome. The $Aβ_{42}$ peptide with 42 amino acids has been shown to be highly susceptible to aggregation and toxic behavior among all the Aβ peptides (36–43)[3–5]. The aggregation process of Aβ peptides leads to formation of polymorphic oligomers, protofibrils, and fibrils which individually display a range of cellular toxicities[6]. Initially, Aβ fibrils were considered the neurotoxic form and causative agent of AD, whereas research in the last decade has revealed that oligomers are the most toxic form of Aβ causing oxidative stress, interacting with signaling receptors, disturbing metal homeostasis and disrupting neuronal cell membrane[3,7]. Membrane disruption is one of the major pathway of toxicity induced by Aβ oligomers[8]. Ramamoorthy *et al.* have recently shown that Aβ exhibit two-step mechanism for membrane disruption, i) Aβ interacts with gangliosides present on the cell membrane to form ion channel-like pores and ii) Aβ fibrillization itself induce membrane fragmentation of lipid bilayer[9]. $Aβ_{42}$ aggregates are an attractive biomarker to target for diagnosis and therapeutics of AD. One of the major problems in the diagnosis of AD is the lack of effective methods for the selective detection of $Aβ_{42}$ aggregates. While diagnosis of AD is traditionally based on behavioral tests or cognition in patients, several imaging technologies such as positron emission tomography (PET)[10], magnetic resonance imaging (MRI)[11], and single-photon emission computed tomography (SPECT)[12] have been developed for the detection of $Aβ_{42}$ aggregates. However, these technologies are still limited by several obstacles, like long data acquisition time, radioactive exposure, poor resolution and need of expensive equipment. Optical imaging using fluorescence and colorimetric probes has emerged as a potential alternative technique as it offers real-time, non-radioactive, high-resolution imaging for inexpensive diagnostics and screening of drugs for AD[13–15]. Thioflavin T (ThT) is the most extensively used fluorescence probe for the *in vitro* detection and staining of $Aβ_{42}$ fibrillar aggregates however, it suffers from poor selectivity and often leads to false detection[16,17]. In the past few years, derivatives of oxazine[18], BODIPY[19], curcumin[20], styryl[21] fluorescein[22] and benzothiazole[23] have been developed and used as fluorescence probes for $Aβ_{42}$ fibrillar aggregates, these probe lack selectivity for $Aβ_{42}$ fibrils over other peptide/protein based aggregates.

[1]Bioorganic Chemistry Laboratory, New Chemistry Unit, Jawaharlal Nehru Centre for Advanced Scientific Research, Jakkur P.O., Bengaluru 560064, Karnataka, India. [2]Division of Theoretical Chemistry and Biology, School of Biotechnology, KTH Royal Institute of Technology, S-106 91 Stockholm, Sweden. Correspondence and requests for materials should be addressed to T.G. (email: tgraju@jncasr.ac.in)

An ideal fluorescence probe must exhibit certain characteristic properties to be used as a diagnostic probe for $A\beta_{42}$ fibrillar aggregates in AD viz., i) high specificity and strong binding affinity, ii) emission in the optical window of 500–750 nm with a large Stokes shift, iii) switch-on fluorescence change upon binding with $A\beta_{42}$ fibrillar aggregates, and iv) ability to rapidly cross the blood brain barrier (BBB). Further, mixed dementia is another state in which abnormal characteristics of more than one type of dementia occur simultaneously and in such cases, determining the specific type of neurodegenerative disorder in the patient is very crucial. Therefore, there is an urgent need for developing probes which could selectively differentiate toxic aggregates responsible for specific neurodegenerative disease. Unfortunately, there is lack of studies on probes that selectively differentiate plaques responsible for any specific disorder. We lack fluorescence probes which selectivity binds to specific aggregates, as most of them fluoresce upon binding to forced or artificially formed protein aggregates generally observed in all kinds of dementia[24]. Recently, J. Yang *et al.* reported an amino naphthalene 2-cyanoacrylate based fluorescence probe, which discriminates between Aβ and Prion plaques by means of differential mode of binding attributed to microenvironments in the binding pockets[25]. However, still there is a need for many more probes which can selectively differentiate other important neurodegenerative disorders. Oligomers being the most toxic form of Aβ causing neuronal death in AD, much efforts are devoted towards studying its structure and designing probes for detection of oligomers. Recently, Knowles *et al.* revealed that the formation of Aβ oligomers depends on the amount of both Aβ monomers and Aβ fibrils. Initially, Aβ aggregates formed through primary nucleation where Aβ monomers self-assemble to fibrils through oligomers as intermediate state. Once a certain concentration of Aβ fibrils is reached they act as secondary nucleation site and initiate the formation of Aβ oligomers from the monomers on their surface this phenomenon is called as secondary nucleation[26]. Therefore designing inhibitors and probes for both Aβ fibrils and oligomers are essential for treating AD and studying its progression[27–29]. Colorimetric detection of $A\beta_{42}$ fibrillar aggregates using antibodies has been demonstrated, but this technique is complicated and expensive[30]. With this background, the need for developing selective fluorometric and colorimetric probes based on simple organic molecules which are easy to handle and offer quick detection is strongly indicated. In this context, we report a hemicyanine derivative as a high affinity, selective, switch-on red fluorescence and colorimetric probe **TC** for $A\beta_{42}$ fibrillar aggregates. **TC** exhibits better detection properties over previously reported fluorescent probes (Table S1).

Results and Discussion

ThT has been extensively used to stain $A\beta_{42}$ fibrillar aggregates for the past few decades. This probe mainly consists of electron donating (N,N-dimethylaniline) and electron withdrawing (benzothiazole) moieties. The benzothiazole group is known to play a crucial role in the interaction of ThT on the surface of $A\beta_{42}$ fibrillar aggregates[31,32]. The major drawbacks of ThT and many other probes involves lack of selectivity and low affinity, which encouraged us to search for a new, more effective fluorescence probe for $A\beta_{42}$ fibrillar aggregates based on the benzothiazole platform, with high selectivity and affinity. We chose to investigate the hemicyanine-based (benzo)thiazole-coumarin (**TC**) conjugate as a 'fluorescence-ready' probe for $A\beta_{42}$ fibrillar aggregates (Fig. 1). A benzothiazole conjugate with hydrophobic pyrene chromophore (**TP**) was also included in our studies (Fig. S1). These compounds are recently reported by our team and discovered **TC** as an effective switch-on red fluorescence probe for DNA containing AT sequences [33]. To our surprise, **TC** with benzothiazole and coumarin moieties was found to exhibit highly enhanced fluorescence with superior selectivity and sensitivity for $A\beta_{42}$ aggregates with higher affinity compared to DNA. Furthermore, the **TC** and **TP** probes with molecular weights in the optimum range of ~350–550 Da, and possesses appropriate log P values and number of hydrogen bond donors and acceptors (Fig. S1)[34].

Initially we studied the molecular interactions of **TC** and **TP** in the absence and presence of $A\beta_{42}$ aggregates through the absorption and emission measurements in PBS buffer (10 mM, pH = 7.4). Mature $A\beta_{42}$ fibrillar aggregates were prepared following the procedure reported in the literature (Supplementary Information). **TC** and **TP** showed absorption bands at 537 nm and 460 nm, respectively, and very weak emissions at 638 nm and 623 nm, respectively, in the absence of $A\beta_{42}$ fibrillar aggregates (Figs 1b and S1). In the presence of $A\beta_{42}$ fibrillar aggregates (10 μM), **TC** (2 μM) showed a remarkable increase in the absorption maxima (hyperchromicity) with an enormous bathochromic shift ($\Delta\lambda_{max} \approx 59$ nm) relating to solution color change from pale pink to purple (Fig. 2). To elucidate the observed spectral changes of **TC**, we carried out concentration-dependent studies of $A\beta_{42}$ fibrillar aggregates against a fixed concentration of **TC** (2 μM). Initially, **TC** exhibited a decrease in absorption intensity in the concentration range 0–1 μM of $A\beta_{42}$ fibrillar aggregates. In addition, a shoulder band was observed for 0.8 μM of $A\beta_{42}$ at 595 nm. Further, with increasing concentration of $A\beta_{42}$ fibrillar aggregates (1–10 μM) the shoulder band at 595 nm became more prominent with strong absorption (Fig. 2a). The bathochromic shift in the absorption band of **TC**, in the presence of $A\beta_{42}$ fibrillar aggregates indicated their favorable interactions. The observed colorimetric change (pale pink to purple) as a consequence of binding of **TC** to $A\beta_{42}$ fibrillar aggregates may be attributed to aggregate-induced changes in the intramolecular alignment and electronic structure of **TC** (Fig. 1)[35,36]. In similar absorption studies with $A\beta_{42}$ fibrillar aggregates, **TP** failed to exhibit any detectable change in absorption and in the color of the solution.

In order to characterize the aggregate-specific shift in the absorption spectrum of **TC** and to propose its absorption maximum as a "colorimetric signature" for amyloidosis, its one photon absorption properties were computed by employing time-dependent density functional theory (at the B3LYP/TZVP level) in polar, non-polar and fibril-like environments. In particular static and dynamic results were presented where the former one involves a single optimized geometry of **TC** in the specific solvent environments while the latter results are obtained as average over numerous configurations from Car-Parrinello QM/MM molecular dynamics. These models are respectively referred to as TD-DFT/PCM and TD-DFT/MM[37]. For further details, we refer to the computational details section of supplementary Information. The calculation only for the most stable binding mode of **TC** in fibril as shown in Fig. 1c has been carried out. Representative snapshots used in TD-DFT/MM calculations

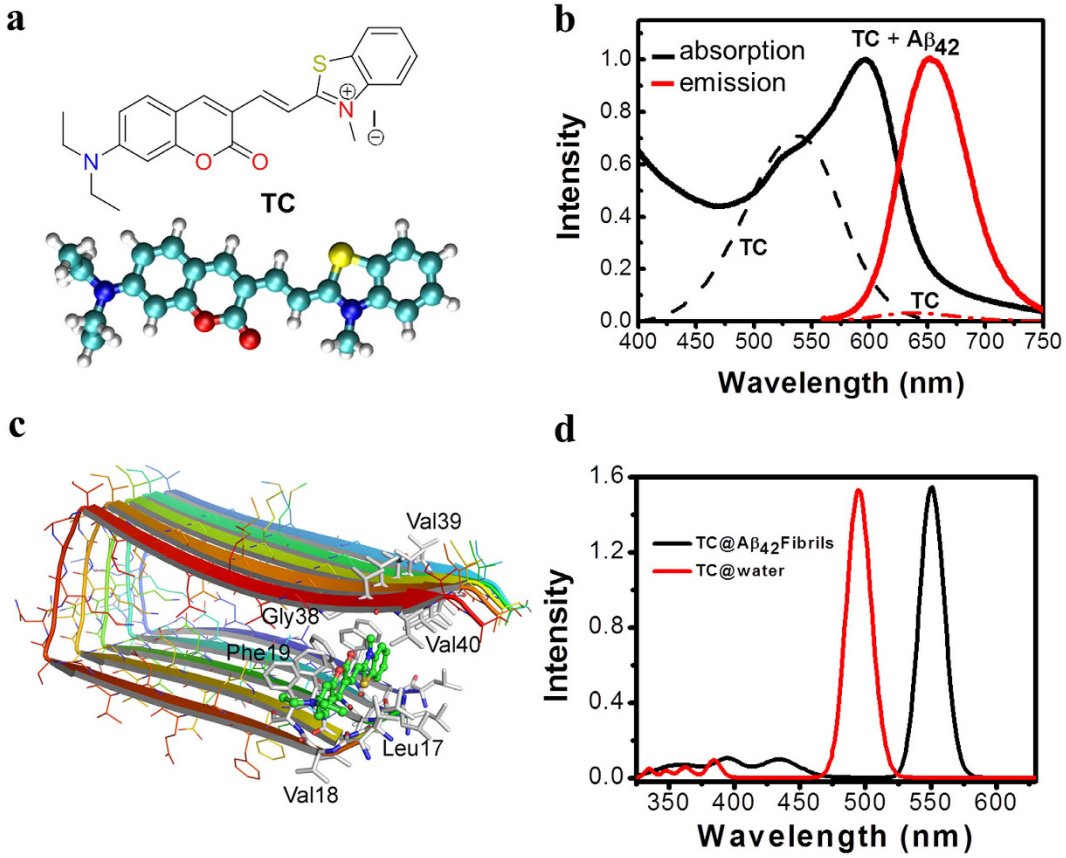

Figure 1. (**a**) Molecular and energy minimized structures of probe **TC**. (**b**) Absorption and emission ($\lambda_{ex} = 537$ nm) spectra of probe **TC** in presence and absence (doted lines) of $A\beta_{42}$ fibrillar aggregates. (**c**) The binding mode of **TC** in the entry site of $A\beta_{42}$ fibril. The $A\beta_{42}$ fibril is shown in cartoon mode, the binding site residues in stick mode and **TC** in stick and ball mode (PyMol 1.3). (**d**) The absorption spectra computed for **TC**@water and **TC**@$A\beta_{42}$ fibril system using TD-DFT/MM models.

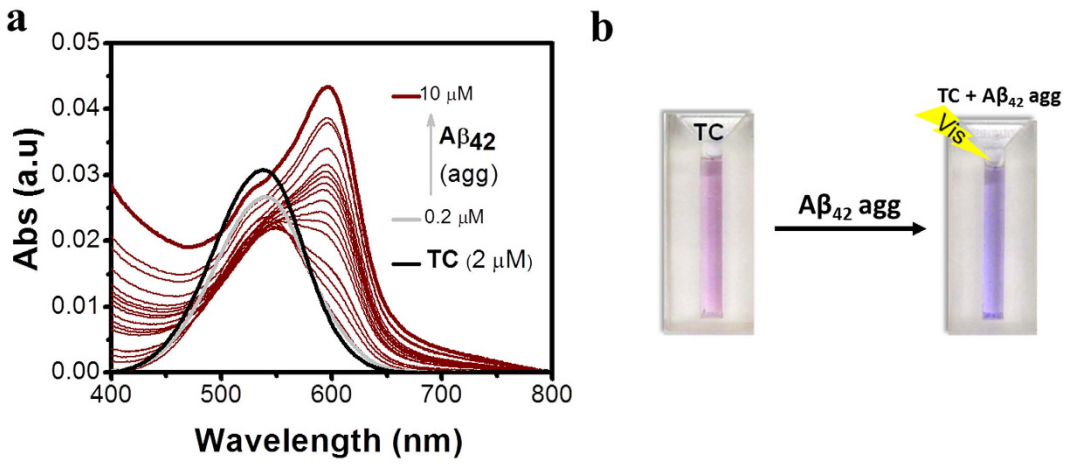

Figure 2. (**a**) Absorption (Abs) spectra of probe **TC** (2 μM) with increasing concentration of $A\beta_{42}$ fibrils (0.2, 0.4, 0.6, 0.8, 1.0, 1.2, 1.4, 1.6, 1.8, 2.0, 2.5, 3.0, 3.5, 4.0, 4.5, 5.0, 6.0, 7.0 and 10.0 μM). (**b**) Photographs of **TC** (2 μM) and **TC** (2 μM) + $A\beta_{42}$ fibrils (15 μM) showing a colorimetric change from pale pink to purple.

for **TC**/fibril and **TC**/water systems are shown in Fig. S2. The spectra computed only for dynamic models (by convoluting the absorption bands of six lowest energy excitations) are shown in Fig. 1d. The absorption spectrum is characterized by a single dominant band in the visible region which is due to the lowest frequency excitation

Method	TC/chloroform	TC/fibril	TC/water	Shift, nm
Static (TD-DFT/PCM)	528(1.9)	–	514 (1.8)	14
Dynamic (TD-DFT/MM)	–	551 (1.6)	495 (1.5)	56
Experiment	561	595	537	58

Table 1. The absorption maximum in nm (with oscillator strength shown in parenthesis) for TC in different micro-environment as predicted from TD-DFT/PCM, and TD-DFT/MM approaches.

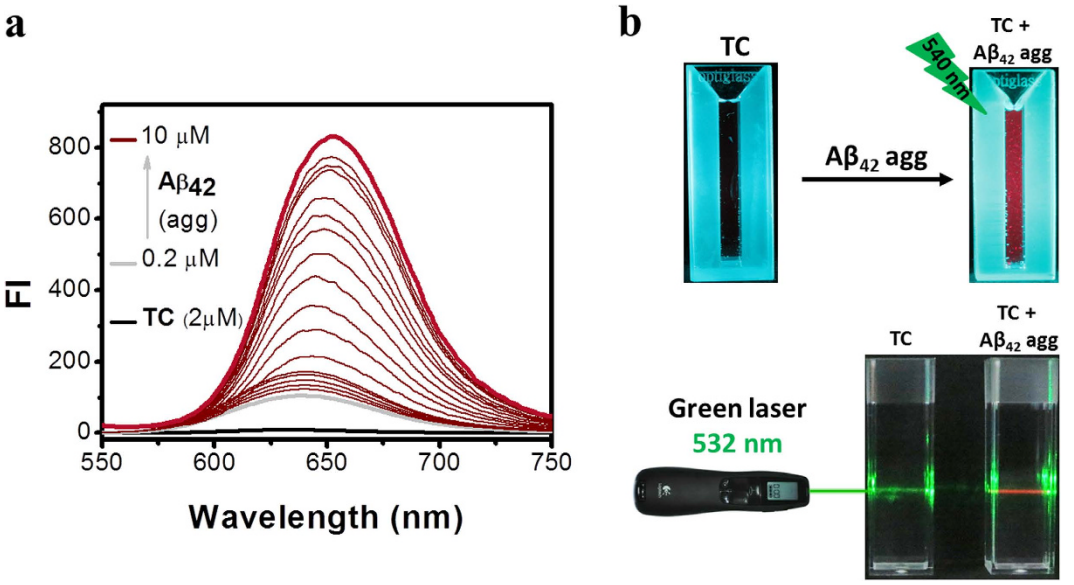

Figure 3. (**a**) Emission (FI) spectra ($\lambda_{ex} = 537$ nm) of probe **TC** (2 μM) with increasing concentration of $A\beta_{42}$ fibrils (0.2, 0.4, 0.6, 0.8, 1.0, 1.2, 1.4, 1.6, 1.8, 2.0, 2.5, 3.0, 3.5, 4.0, 4.5, 5.0, 6.0, 7.0 and 10.0 μM). (**b**) Photographs of **TC** and **TC** (2 μM) + Aβ42 (15 μM) fibrils samples illuminated under green light (540 nm), **TC** (2 μM) + $A\beta_{42}$ (15 μM) illuminated with laser emitting green light (532 nm) shows a red beam in the sample solution.

of π-π^* character. The molecular orbitals involved in this excitation are shown in the supplementary information (Fig. S3). The absorption maximum (λ_{max}) for **TC** from the aforementioned models is listed in Table 1 along with the experimental results which show a red shift by 58 nm for the **TC** probe going into the fibril-like environment.

The simplistic polarizable continuum model reproduces the trend of a red-shift in the absorption spectra of **TC** when going from water-like to non-polar, chloroform environment even though the size of the shift is small (14 nm) when compared to experiment (24 nm). Based on this result, it can be suggested that the hydrophilic-like to hydrophobic-like change in the micro-environment may be a feasible mechanism for the fibril-induced red-shift in the absorption spectra of **TC**. The more sophisticated TD-DFT/MM approach which accounts for electrostatic and polarization interactions between **TC** and its fibril-like and aqueous environment also confirmed this and reproduce the red shift (56 nm) in excellent agreement with experiment. Usually, the change in the micro-environment alters the molecular structure and conformation of the probe which also significantly contributes to the shift in the spectra[38]. For this reason, we investigated the fibril-induced changes in conformation and molecular structure (along the conjugation pathway) of **TC** and interestingly, this does not change significantly (refer to section 3.0 of the supplementary Information) and so only contributes to the shift by 4 nm. The absolute λ_{max} is underestimated in our model which refers to limitations of the QM model itself. Our motivation though, is to explain the possible origin for the observed red shift due to change in environment (aqueous to fibril), something that is allowed by the excellent reproduction of the red shift by the more advanced TD-DFT/MM model. The characterization of the micro-environment of **TC** binding site clarifies its hydrophobic nature, and we can attribute the change in the hydrophilic-like to hydrophobic-like environment around **TC** when it binds to the fibril as the responsible factor for the red shift.

Subsequently, we performed fluorescence titration experiments to probe the response of **TC** in the presence of $A\beta_{42}$ fibrillar aggregates. The emission spectrum of **TC** (2 μM) exhibited a ~30-fold fluorescence enhancement ($E_{max} = 654$ nm) when bound to $A\beta_{42}$ fibrillar aggregates. The quantum yield of probe **TC** alone in PBS (10 mM) is 0.073, while **TC** bound to $A\beta_{42}$ fibrillar aggregates showed appreciable quantum yield of 0.40 (Fig. 3). Again, **TP** did not show any detectable change in the fluorescence behavior in the presence of $A\beta_{42}$ fibrillar aggregates. The switch-on red fluorescence of **TC** is a typical behavior of cyanine-based probes, which are known to form twisted intramolecular charge transfer (TICT) complexes in the excited state and exhibit fluorescence emission in response to a surrounding environment[39]. **TC** probe alone is non-fluorescence in buffer due to internal non-radiative molecular twisting and self-aggregation, whereas the intramolecular twisting is restricted upon binding to $A\beta_{42}$

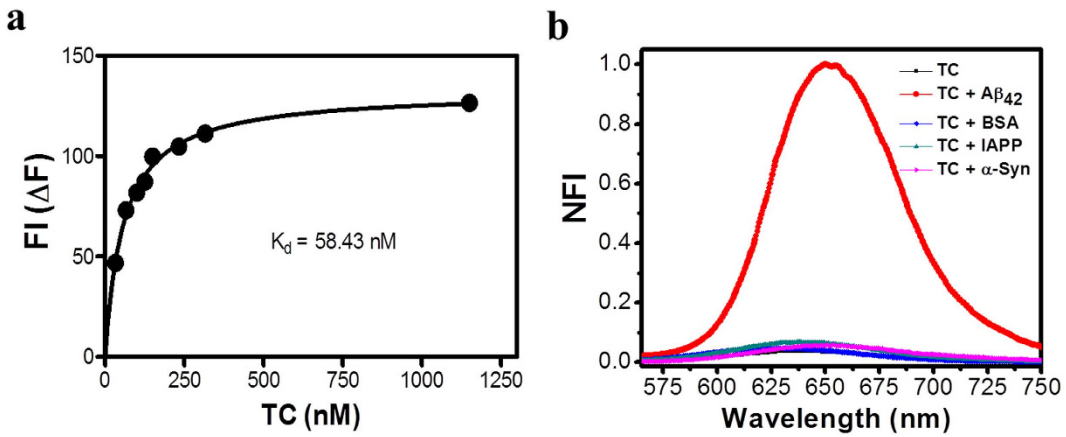

Figure 4. (**a**) Plot of the difference in fluorescence intensity (ΔF) as a function of the concentration of **TC** in the presence of $A\beta_{42}$ fibrillar aggregates (2 μM) in solutions (10 mM PBS). (**b**) Normalized fluorescence intensity (NFI) of **TC** upon interaction with aggregates of $A\beta_{42}$ (5 μM), α-synuclein (α-Syn) (20 μM), amylin (IAPP) (20 μM) and hydrophobic protein bovine serum albumin (BSA).

fibrillar aggregates leading to enhanced (~30-fold) red fluorescence[40,41]. $A\beta_{42}$ fibrillar aggregates (30 μM) were incubated with ThT (5 μM) and **TC** (5 μM) for 5 min and imaged under fluorescence microscope. Characteristic $A\beta_{42}$ fibrillar aggregates can be distinctly seen in TEM images, whereas fluorescence images show large clumps of $A\beta_{42}$ aggregates owing to low resolution of the technique (Fig. S7). Probe **TC** did not show appreciable changes in the absorption and emission properties under different buffer conditions which indicate that solvent (buffer solution) has no significant effect on the conformational or aggregation tendency of the probe (Fig. S4). Furthermore, a pH-dependent study showed that photophysical properties of probe **TC** is not affected in the pH range of 3–8, which reaffirm the utility of the probe in most physiological conditions (Fig. S5).

Next, we calculated the binding constant by studying the fluorescence response with varying concentration of **TC** against a fixed concentration of $A\beta_{42}$ fibrillar aggregates (dose-dependent saturation assay, Fig. S8). The obtained standard saturation curve was fitted to a single-binding site, which gave a dissociation constant K_d of 58 ± 1.2 nM (the association constant was calculated to be $K_a = 1.72 \times 10^7\,M^{-1}$ for 2 μM of $A\beta_{42}$ fibrillar aggregates) (Fig. 4a). Notably, our recent study showed that AT-selective binding of **TC** to a DNA duplex generates a ~16-fold fluorescence enhancement and K_d in the micromolar range (10 μM)[33]. Remarkably, the current study reveals a ~30-fold fluorescence enhancement with K_d in the nanomolar range indicating a much higher binding affinity of **TC** towards $A\beta_{42}$ fibrillar aggregates compared to DNA[42]. To further evaluate high affinity of **TC** towards $A\beta_{42}$ fibrillar aggregates compared to DNA, we have performed a competitive binding experiment. The competitive binding experiment is based on the fact that, when **TC** binds to either $A\beta_{42}$ fibrillar aggregates or DNA show characteristic changes in both absorption and emission spectra corresponding to probe **TC** and changes observed in each case are substantially different. First, probe **TC** was saturated with excess DNA (calf thymus) which showed characteristic changes in both absorption and emission spectra of **TC**, which corresponds to DNA binding, but when the same sample was added with $A\beta_{42}$ fibrillar aggregates (10 μM, incubate for 15 min), it exhibited changes in both absorption and emission spectra which were similar to absorption and emission features corresponding to **TC** bound to $A\beta_{42}$ fibrillar aggregates alone. This observation highlights the fact that in the presence of both $A\beta_{42}$ fibrillar aggregates and DNA it preferably binds to $A\beta_{42}$ fibrillar aggregates over DNA (Fig. S9). In addition, the K_d of $A\beta_{42}$ fibrillar aggregates bound **TC** is very low compared to that of the control probes ThT (~0.8 μM) and Congo red (~1.1 μM) confirming the superiority of the **TC** probe in terms of binding affinity towards $A\beta_{42}$ fibrillar aggregates[43,44]. Oligomers and fibrils are prominent polymorphic forms of $A\beta_{42}$ aggregates. Probe **TC** showed selective fluorescence enhancement towards $A\beta_{42}$ fibrils over oligomers which exhibited a slight red shift (8 nm) in the basal fluorescence and negligible fluorescence enhancement (Fig. S10). Further we have performed fluorescence studies in the presence of intracellular protein content bovine serum albumin (BSA), fibrillar aggregates of α-synuclein (α-Syn) and islet amyloid polypeptide (IAPP, amylin) implicated in Parkinsons disease and type II diabetes, respectively. Incubation of **TC** with BSA, α-Syn aggregates and IAPP aggregates (20 μM) did not lead to significant fluorescence enhancements confirming the preferential selectivity of the probe towards $A\beta_{42}$ fibrillar aggregates over other proteins and peptide aggregates (Fig. 4b).

Recently, Suzuki *et al.* have studied the competitive binding of Aβ inhibitor, EGCG and ThT towards Aβ aggregates using ^{19}F NMR to understand its binding interactions[45]. Similarly, to gain further insight into the binding interaction of **TC** probe, displacement assay was performed against ThT-bound $A\beta_{42}$ fibrillar aggregates. The well-separated emission spectra of ThT (green region) and **TC** (red region) made it possible to observe fluorescence changes corresponding to individual probes during the displacement experiments (Fig. S12). Remarkably, a gradual addition of **TC** to the ThT/ $A\beta_{42}$ fibrillar aggregate complex (ThT = 5 μM and $A\beta_{42}$ = 10 μM) resulted in a steady decay in fluorescence at 483 nm (λ_{ex} = 450 nm) and a corresponding enhancement in the emission intensity at 654 nm (λ_{ex} = 537 nm). This clearly suggested an effective displacement of ThT by **TC** owing to the formation of a much stronger **TC**/$A\beta_{42}$ fibrillar aggregate complex (Fig. 5a). An interesting observation was made during the titration studies where spectral features corresponding to emission of **TC** (at 654 nm) were observed

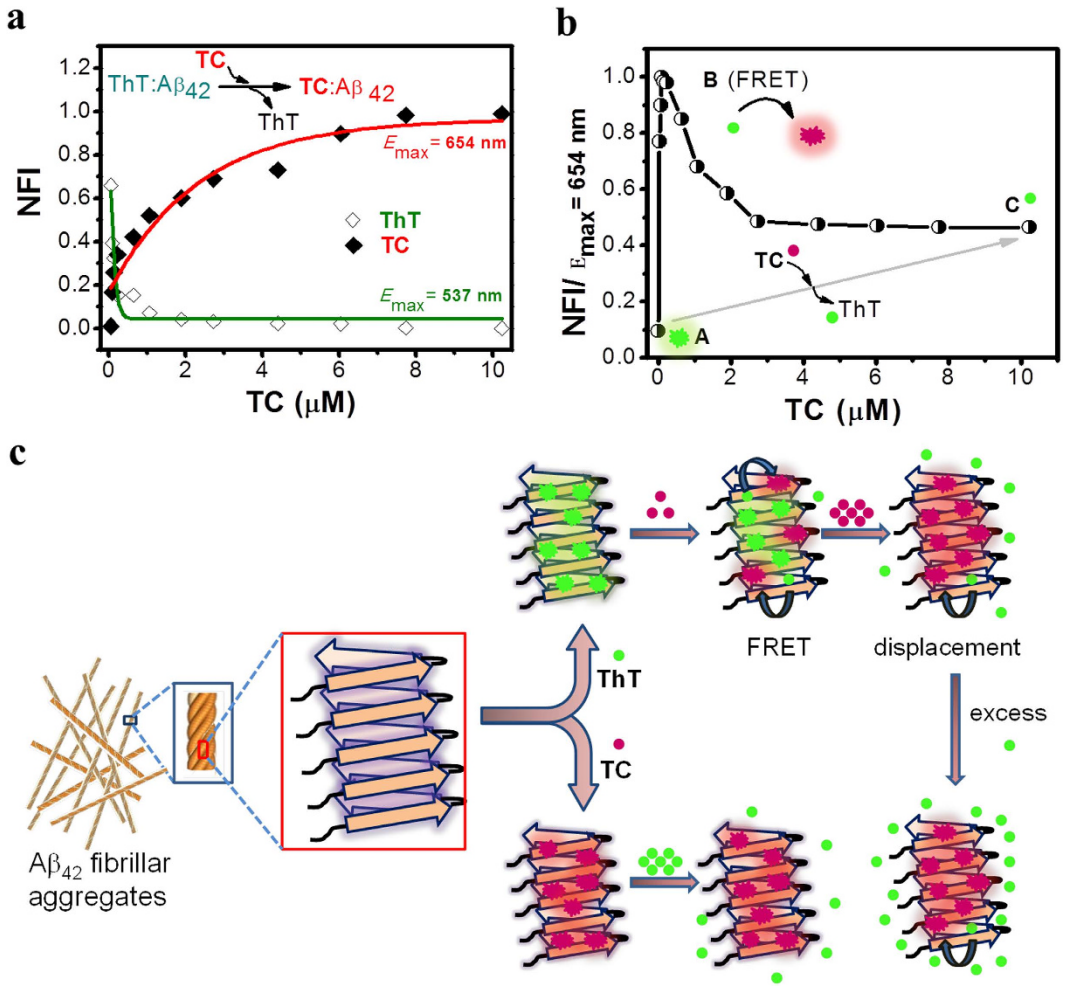

Figure 5. Displacement assay. (**a**) Titration of **TC** to ThT/$A\beta_{42}$ fibrillar aggregate complex (ThT, 5 μM/$A\beta_{42}$ fibrils, 10 μM) in 10 mM PBS buffer solution. High affinity **TC** effectively displaces ThT from the ThT/$A\beta_{42}$ fibrillar aggregate complex, as monitored by the decrese in fluorescence emission at 483 nm (◊ green trace, $\lambda_{ex} = 450$ nm) and corresponding increase in fluorescence emission at 654 nm (♦ red trace, $\lambda_{ex} = 537$ nm). (**b**) In displacement assay (**a**) emission of **TC** monitored at 654 nm (E_{max}) upon excitation at 450 nm (λ_{ex} of ThT). Region A: ThT/$A\beta_{42}$ fibrillar aggregate complex. Region B: **TC**/ThT/$A\beta_{42}$ fibrillar aggregate complex, at low concentration **TC** coexists with ThT leading FRET between them. Region C: **TC** displaces ThT, with residual ThT (possibaly in the inner cleft of the $A\beta_{42}$ fibril) which leads to residual FRET. (**c**) Proposed model for the **TC** displacement of ThT and FRET between them on the $A\beta_{42}$ fibrils. NFI: Normalized fluorescence intensity.

upon excitation of the sample (**TC**/ThT/$A\beta_{42}$ fibrillar aggregates) at 450 nm (ThT excitation wavelength). Addition of **TC** (33 nM to 10.233 μM) to the ThT/ $A\beta_{42}$ fibrillar aggregate complex showed a gradual decrease in the fluorescence emission at 483 nm (ThT) as expected. However, upon 450 nm (ThT) excitation, fluorescence was also observed at 654 nm (**TC**) with a slight red shift. The fluorescence intensity of this unprecedented emission band (**TC**) decreased slowly with further increase in the concentration of added **TC** and finally reached a constant value (Fig. 5b). These changes in the emission characteristics, particularly the fluorescence emission of **TC** upon excitation corresponding to ThT is attributed to fluorescence resonance energy transfer (FRET) between the $A\beta_{42}$ fibrillar aggregates bound to ThT and **TC**. Evidently, the emission spectrum of ThT significantly overlaps with the absorption spectrum of **TC** making them a suitable donor-acceptor pair on the aggregate surface (Fig. S12)[46,47]. At the beginning of the titration, **TC** binds to the ThT/$A\beta_{42}$ fibrillar aggregates complex by partially displacing ThT, leading to FRET between bound ThT (donor) and **TC** (acceptor) (Fig. 5b). For concentrations of **TC** > 150 nM, displacement of ThT by **TC** resulted in a decreased FRET-fluorescence of **TC** (Fig. S6). However, the FRET-based fluorescence at 654 nm was not quenched completely due to persistent residual ThT-**TC** pairs on an $A\beta_{42}$ fibrillar aggregates. The quenching of fluorescence intensity of ThT (at 483 nm) to its basal level indicates that **TC** binds to similar primary binding pockets of $A\beta_{42}$ fibrillar aggregates occupied by ThT. On the other hand, excitation at 537 nm (**TC**) showed a gradual increase in fluorescence independent of ThT displacement, confirming the presence of multiple binding sites for **TC** on $A\beta_{42}$ fibrillar aggregates (Fig. 6). The displacement of ThT was almost instantaneous and did not require any incubation time. Addition of **TC** (1 μM) to the ThT (10 μM)/$A\beta_{42}$ (50 μM) complex led to a complete change in emission color of the sample, from green to bright pinkish red, as seen under

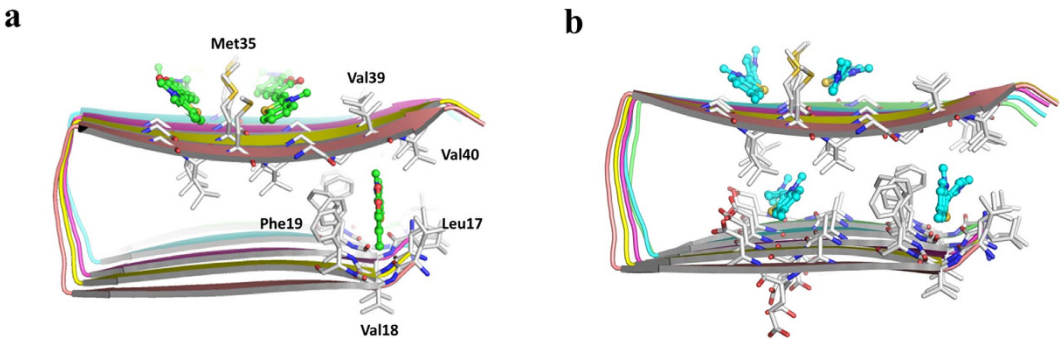

Figure 6. Docking results of (**a**) **TC** and (**b**) ThT with $A\beta_{42}$ fibril (all binding sites are shown). The fibril is shown in cartoon mode, the binding site residues in stick mode and **TC** or ThT in stick and ball mode.

UV-light illumination ($\lambda_{ex} = 365$ nm). Addition of excess ThT (50 μM) did not displace **TC** from its complex with $A\beta_{42}$ fibrillar aggregates owing to the high binding constant (Fig. S13). The $A\beta_{42}$ fibrillar aggregates stained with **TC** retained red fluorescence even after 50 days of aging, thus further indicating the strong binding affinity and non-dissociative nature of **TC** upon binding to $A\beta_{42}$ fibrillar aggregates.

In order to get a microscopic picture of the **TC** to fibril binding, we carried out a molecular docking study. In agreement with experimental indications, our study shows that there are multiple binding sites (such as entry cleft and surface) in the fibril accessible for binding of **TC** (Fig. 6). However, the most favorable binding site was identified in the entry site formed by Leu17, Val18, Phe19, Gly38, Val39 and Val40 (Fig. 1c). The binding affinity calculated by AutoDock is the highest in this site (about −8.5 kcal/mol), whereas in other sites, it is in the range of −6.0 ~ −8.0 kcal/mol. A flexible molecular model for **TC** during the docking yields a binding affinity equivalent to −9.86 kcal/mol which corresponds to $K_d = 55.5$ nM (which is in good agreement with experimental data). As **TC** is positively charged, it is unfavorable to bind in the inner sites which are fully buried, and the partially buried entry site is more favorable. Figure 1c shows that **TC** is clamped in the entry site mainly through hydrophobic interaction with Leu17 and Val39 through π-π stacking interaction with the phenyl ring of Phe19. Water molecules can also enter this site to solvate the positive charge of **TC**. It is relevant to note that all the amino acids form this binding pocket are hydrophobic and hence we believe that the red shift in the spectra is due to the change from hydrophilic to hydrophobic like micro-environment around the probe. Further, the bulky nature of the diethyl amino group makes it impossible for the **TC** probe to become buried inside the binding site, rather it is partly exposed to the solvent environment (Fig. S3a). Figure 6a,b show all possible binding sites available for **TC** and ThT in the fibril. The **TC** binds to the entry cleft, inner core and surface binding sites while **TC** binds only to the entry cleft and the surface binding sites which have to be attributed to the larger van der Waals surface associated with the latter molecule. Due to the larger binding affinity of **TC** towards the amyloid peptide, it can replace the ThTs in the entry cleft and other surface binding sites (which is supported by FRET data). However, ThTs in the core sites cannot be displaced by **TC**s and these therefore contribute to the population of residual that-**TC** pairs on $A\beta_{42}$ aggregate contributing to the significant FRET intensity as discussed above. Additionally, we performed docking studies of **TC** with α-synuclein (PDB code: 4R0U) and IAPP (PDB code: 2KIB) fibrils[48,49]. It is found that **TC** can only be docked to the surface or the flanks of these two fibrils. It cannot be docked into the core sites (in particular to entry cleft site) as in the case of the $A\beta_{42}$ fibril. The docking scores (empirical binding free energies) of **TC** with α-synuclein and IAPP are in the range between −5.0 ~ −7.0 kcal/mol, which are much lower (in terms of magnitude) than that with the $A\beta_{42}$ fibril in the entry site (−8.5 kcal/mol). This result suggests that **TC** binds much more favorably with $A\beta_{42}$ fibril than with α-synuclein and IAPP (Fig. S14).

Conclusion

We demonstrated that the hemicyanine-based benzothiazole-coumarin (**TC**) probe binds to $A\beta_{42}$ aggregates with nanomolar affinity ($K_a = 1.72 \times 10^7 M^{-1}$). The probe showed switch-on red fluorescence with a large Stokes shift (~117 nm) upon binding to $A\beta_{42}$ aggregates along with a characteristic colorimetric response which can be attributed to a change in the dielectric nature of the micro-environment around **TC** from hydrophilic-like to hydrophobic-like. The **TC** probe also showed good specificity as it did not interact with other abnormal protein aggregates of α-Syn and IAPP. Owing to high binding affinity, the **TC** probe displaced the ThT probe bound to $A\beta_{42}$ aggregates, conversely very high concentrations of ThT could not displace **TC** bound to $A\beta_{42}$ aggregates. The binding site in the $A\beta_{42}$ fibril for **TC** has been revealed from molecular docking studies. We propose that optimization of **TC** as a lead probe for $A\beta_{42}$ aggregates may afford novel, useful optical-based diagnostic probe for Alzheimer's disease.

Methods

All reagents and solvents were obtained from Sigma-Aldrich and used without further purification. All air and moisture sensitive reactions were carried out under an argon atmosphere. Absorption spectra were recorded with Perkin Elmer Model Lambda 900 spectrophotometer. Fluorescence spectral measurements were carried out by using Perkin Elmer Model LS 55 fluorescence spectrophotometer. Incubation for fibril formation was performed in the Eppendorf Inova42 incubator.

Synthesis of probes. Probes **TC** and **TP** were synthesized following the literature procedure recently reported from our group[33].

Preparation of $A\beta_{42}$ fibrillar aggregates[50]. $A\beta_{42}$ peptide (0.25 mg) (Merck, calbiochem) was dissolved in hexafluoro-2-propanol (HFIP, 0.2 mL) and incubated at room temperature for 1 h. HFIP was then removed by a flow of nitrogen and further dried by vacuum. HFIP-treated $A\beta_{42}$ was then dissolved in DMSO to a final concentration of 1 mM and diluted to 200 μM with 10 mM PBS buffer (pH 7.4). The solution was incubated at 37 °C for 48 h with gentle and constant shaking. The formation of $A\beta_{42}$ fibrillar aggregates was confirmed by ThT assay, CD measurements and TEM (Fig. S11).

Preparation of amylin (IAPP) fibrillar aggregates and α-Synuclein fibrils[51,52]. Amylin peptide (0.1 mg) (Merck, calbiochem) sample of was dissolved in 100 μL of acetonitrile to disrupt any pre-existing aggregates, and taken up in 200 μL of 10 mM PBS buffer (pH 7.4). The final concentration of acetonitrile in the fibrillization buffer was 10% (v/v). The solution was sonicated continuously for 1 min to break up any potential aggregates. To form fibrils, the sample was incubated at 37 °C without agitation in an eppendorf tube for 120 h (5 days). α-Synuclein peptide (0.5 mg) (Sigma-Aldrich) was dissolved in hexafluoro-2-propanol (HFIP, 0.2 mL) and incubated at room temperature for 1 h. HFIP was then removed by a flow of nitrogen and further dried by vacuum. Then α-Synuclein peptide is dissolved TBS buffer to a concentration of 200 μM. Then the solution is incubated at 37 °C for 3–5 days with constant shaking of 150 rpm.

Determination of the binding constant of TC for $A\beta_{42}$ aggregates[19]. Increasing concentration of probe **TC** (0–1.15 μM) was titrated against a fixed concentration of $A\beta_{42}$ aggregates (2 μM) and fluorescence intensity at 639 nm was recorded ($\lambda_{ex} = 537$ nm). The K_d binding curve was generated by GraphPad Prism 5.0 (GraphPad Software, Inc., La Jolla, CA, USA) by using below equation, where X is concentration of probe **TC** and Y is change in fluorescence intensity

$$Y = B_{max}{}^{*}X/(K_d + X)$$

B_{max} is the maximum specific binding has the same units as Y.
K_d is the equilibrium binding constant.

Molecular Docking. Molecular docking was performed using AutoDock 4.2, and the AutoDock-Tools software was used to set up the necessary inputs for the docking program[53]. The structure of fibril consisting of 5 $A\beta_{42}$ peptides (PDB code 2BEG)[54] was taken from the Protein Data Bank and was used as the protein model for docking in this study. The geometry of **TC** in gas phase was optimized at the level of B3LYP/6–31+G* using the Gaussian09 software. A grid box centered on the protein was defined with a dimension of $90 \times 70 \times 60$ Å using a 0.375 Å grid step, which is large enough to encompass the whole protein and leave enough space for docking ligand on the surface. The Lamarckian Genetic Algorithm was used for legend conformation, search and was run for 100 times, which would generate 100 possible protein-ligand complexes. All other parameters were left as default. The resulting ligand conformers were clustered by root mean square deviation (RMSD).

References

1. Ferri, C. P. *et al.* The global prevalence of dementia: A systematic review and metaanalysis. *Alzheimer's & Dementia* **9,** 63–75 (2013).
2. Sink, K. M., Holden, K. F. & Yaffe, K. Pharmacological treatment of neuropsychiatric symptoms of dementia. *JAMA* **293,** 596–608 (2005).
3. Rajasekhar, K., Chakrabartia, M. & Govindaraju T. Function and toxicity of amyloid beta and recent therapeutic interventions targeting amyloid beta in Alzheimer's disease. *Chem. Comm.* **51,** 13434–13450 (2015).
4. Savelieff, M. G. *et al.* Untangling amyloid-β, Tau, and metals in Alzheimer's disease. *ACS Chem. Biol.* **8,** 856–865 (2013).
5. De Toma, A. S., Salamekh, S., Ramamoorthy, A. & Lim, M. H. Misfolded proteins in Alzheimer's disease and type II diabetes. *Chem. Soc. Rev.* **41,** 608–621 (2012).
6. Berhanu, W. M. & Hansmann, U. H. E. Structure and dynamics of amyloid-β segmental polymorphisms. *PLoS ONE* **7,** e41479 (2012).
7. Kotler, S. A. *et al.* High-resolution NMR characterization of low abundance oligomers of amyloid-β without purification. *Sci. Rep.* **5,** 11811 (2015).
8. Kotler, S. A. *et al.* Differences between amyloid-β aggregation in solution and on the membrane: insights into elucidation of the mechanistic details of Alzheimer's disease. *Chem. Soc. Rev.* **43,** 6692–6700 (2014).
9. Sciacca, Michelea F. M. *et al.* Two-step mechanism of membrane disruption by Aβ through membrane fragmentation and pore formation. *Biophys. J.* **103,** 702–710 (2012).
10. Henriksen, G., Yousefi, B., Drzezga, A. & Wester, H. J. Development and evaluation of compounds for imaging of β-amyloid plaque by means of positron emission tomography. *Eur. J. Nucl. Med. Mol. Imaging* **35,** 75–81 (2008).
11. Wengenack, T. M. *et al.* Design and chemical synthesis of a magnetic resonance contrast agent with enhanced *in vitro* binding, high blood-brain barrier permeability, and *in vivo* targeting to Alzheimer's disease amyloid plaques. *Biochemistry* **43,** 6064–6075 (2004).
12. Saji, H. *et al.* Radioiodinated benzimidazole derivatives as single photon emission computed tomography probes for imaging of β-amyloid plaques in Alzheimer's disease *Nucl. Med. Biol.* **38,** 313–320 (2011).
13. Selkoe, D. J. Imaging Alzheimer's amyloid. *Nat. Biotechnol.* **18,** 823−824 (2000).
14. Hamachi, I. *et al.* Fluorescent BODIPY-based Zn(II) complex as a molecular probe for selective detection of neurofibrillary tangles in the brains of Alzheimer's disease patients. *J. Am. Chem. Soc.* **131,** 6543–6548 (2009).
15. Staderini, M., Martin, M. A., Bolognesi, M. L. & Menendez, J. C. Imaging of β-amyloid plaques by near infrared fluorescent tracers: a new frontier for chemical neuroscience. *Chem. Soc. Rev.* **44,** 1807–1819 (2015).
16. Xiong, Y. *et al.* Protein-induced photophysical changes to the amyloid indicator dye thioflavin T. *Proc. Natl. Acad. Sci. USA* **107,** 16863–16868 (2010).
17. Robbins, K. J., Liu, G., Selmani, V. & Lazo, N. D. Conformational analysis of Thioflavin T bound to the surface of amyloid fibrils. *Langmuir* **28,** 16490−16495 (2012).

18. Gremlich, H. *et al. In vivo* detection of amyloid-β deposits by near-infrared imaging using an oxazine-derivative probe. *Nat. Biotechnol.* **23,** 577−583 (2005).
19. Ono, M., Watanabe, H., Kimura, H. & Saji, H. BODIPY-based molecular probe for imaging of cerebral β-Amyloid plaques. *ACS Chem. Neurosci.* **3,** 319–324 (2012).
20. Zhang, S. *et al.* Bivalent ligand containing curcumin and cholesterol as a fluorescence probe for Aβ plaques in Alzheimer's disease. *ACS Chem. Neurosci.* **3,** 141–146 (2011).
21. Levine, H. Mechanism of Aβ(1–40)fibril-induced fluorescence of (*trans*, *trans*)-1-bromo-2,5-bis(4-hydroxystyryl)benzene (K114). *Biochemistry* **44,** 15937–15943 (2005).
22. Muthuraj, B., Layek, S., Balaji, S. N., Trivedi, V. & Iyer, P. K. Multiple function fluorescein probe performs metal chelation, disaggregation, and modulation of aggregated Aβ and Aβ-Cu complex. *ACS Chem. Neurosci.* (2015).
23. Jameson, L. P., Smith, N. W. & Dzyuba, S. V. Dye-binding assays for evaluation of the effects of small molecule inhibitors on amyloid (Aβ)self-assembly. *ACS Chem. Neurosci*. **3,** 807–819 (2012).
24. Knowles, T. P. J., Vendruscolo, M. & Dobson, C. M. The amyloid state and its association with protein misfolding diseases. *Nature Rev. Mol. Cell Biol*. **15,** 384–396 (2014).
25. Yang, J. *et al.* Aminonaphthalene 2-cyanoacrylate (ANCA)probes fluorescently discriminate between amyloid-β and Prion plaques in brain. *J. Am. Chem. Soc.* **134,** 17338–17341 (2012).
26. Knowles, T. P. J. *et al.* Proliferation of amyloid-β 42 aggregates occurs through a secondary nucleation mechanism. *Proc. Natl. Acad. Sci. USA*. **110,** 9758–9763 (2013).
27. DeToma, A. S. *et al.* Interaction and reactivity of synthetic aminoisoflavones with metal-free and metal-associated amyloid-β. *Chem. Sci*. **5,** 4851–4862 (2014).
28. Lee, S. *et al.* Rational design of a structural framework with potential use to develop chemical reagents that target and modulate multiple facets of Alzheimer's disease. *J. Am. Chem. Soc.* **136,** 299–310 (2014).
29. Savelieff, M. G. *et al.* A small molecule that displays marked reactivity toward copper- versus zinc-amyloid-β implicated in Alzheimer's disease. *Chem. Comm*. **50,** 5301–5303 (2014).
30. Glabe, C. G. *et al.* Fibril specific, conformation dependent antibodies recognize a generic epitope common to amyloid fibrils and fibrillar oligomers that is absent in prefibrillar oligomers. *Mol. Neurodegener.* **2,** 1–8 (2007).
31. Ågren, H. *et al.* Amyloid fibril-induced structural and spectral modifications in the thioflavin-T optical probe. *J. Phys. Chem. Lett.* **4,** 70−77 (2013).
32. Groenning, M. Binding mode of thioflavin T and other molecular probes in the context of amyloid fibrils-current status. *J. Chem. Biol.* **3,** 1–18 (2010).
33. Govindaraju, T. *et al.* A thiazole coumarin (TC)turn-on fluorescence probe for AT-base pair detection and multipurpose applications in different biological systems. *Sci. Rep*. **4,** 6476 (2014).
34. Pajouhesh, H. & Lenz, G. Medicinal chemical properties of successful central nervous system drugs. *Neuro RX*. **2,** 541–553 (2005).
35. Huang, Z. S. *et al.* Development of a universal colorimetric indicator for G-quadruplex structures by the fusion of thiazole orange and isaindigotone skeleton. *Anal. Chem.* **84,** 6288–6292 (2012).
36. Turoverov, K. K. *et al.* Interaction of thioflavin T with amyloid fibrils: fluorescence quantum yield of bound dye. *J. Phys. Chem. B* **112,** 15893–15902 (2008).
37. Olsen, J. M., Aidas, K. & Kongsted, J. Excited states in solution through polarizable embedding. *J. Chem. Theory Comput.* **6,** 3721–3734 (2010).
38. Murugan, N. A., Kongsted, J., Rinkevicius, Z. & Ågren, H. Color modeling of protein optical probes. *Phys. Chem. Chem. Phys.* **14,** 1107–1112 (2012).
39. Grabowski, Z. R., Rotkiewicz, K. & Rettig, W. Structural changes accompanying intramolecular electron transfer: focus on twisted intramolecular charge-transfer states and structures. *Chem. Rev.* **103,** 3899–4032 (2003).
40. Haidekker, M. A. & Theodorakis, E. A. Molecular rotors-fluorescent biosensors for viscosity and flow. *Org. Biomol. Chem.* **5,** 1669–1678 (2007).
41. Theodorakis, E. A. *et al.* Rational design of amyloid binding agents based on the molecular rotor motif. *Chem Med Chem* **5,** 56–60 (2010).
42. Cook, N. P., Ozbil, M., Katsampes, C., Prabhakar, R. & Martí, A. A. Unraveling the photoluminescence response of light-switching Ruthenium(II)complexes bound to amyloid-β. *J. Am. Chem. Soc.* **135,** 10810–10816 (2013).
43. Levine, H. Multiple ligand binding sites on Aβ(1-40)fibrils. *Amyloid* **12,** 5−14 (2005).
44. Lansbury, P. T. *et al.* Synthesis and amyloid binding properties of rhenium complexes: preliminary progress toward a reagent for SPECT imaging of Alzheimer's disease brain. *J. Med. Chem.* **42,** 2805–2815 (1999).
45. Suzuki, Y. *et al.* Resolution of oligomeric species during the aggregation of Aβ40 using ^{19}F NMR. *Biochemistry* **52,** 1903–1912 (2013).
46. Alies, B. *et al.* Concept for simultaneous and specific *in situ* monitoring of amyloid oligomers and fibrils via forster resonance energy transfer. *Anal. Chem*. **86,** 11877–11882 (2014).
47. Erijman, E. J. & Jovin, T. FRET imaging. *Nat. Biotechnol.* **21,** 1387–1395 (2003).
48. Li, D. *et al.* Structure-based design of functional amyloid materials. *J. Am. Chem. Soc*. **136,** 18044–18051 (2014).
49. Nielsen, J. T. *et al.* Unique identification of supramolecular structures in amyloid fibrils by solid-state NMR spectroscopy. *Angew. Chem. Int. Ed.* **48,** 2118–2121(2009).
50. Jan, A., Hartley, D. M. & Lashuel, H. A. Preparation and characterization of toxic Aβ aggregates for structural and functional studies in Alzheimer's disease research. *Nat. Protoc.* **5,** 680–685 (2010).
51. Konarkowska, B., Aitken, J. F., Kistler, J., Zhang, S. & Cooper, G. J. The aggregation potential of human amylin determines its cytotoxicity towards islet β-cells. *FEBS J.* **273,** 3614–3624 (2006).
52. Sigurdsson, W. & Einar, M. *Amyloid proteins: Methods and protocols. Vol. 299*, Springer (2005).
53. Olson, A. J. *et al.* AutoDock4 and AutoDockTools4: Automated docking with selective receptor flexibility. *J. Comput. Chem*. **30,** 2785–2791 (2009).
54. Luhrs, T. Ritter, C. Adrian, M. Riek-Loher, D. & Bohrmann, B. 3D structure of Alzheimer's amyloid-β (1–42) fibrils. *Proc. Natl. Acad. Sci. USA* **102,** 17342–17347 (2005).

Acknowledgements

We thank Prof. C. N. R. Rao FRS for constant support, JNCASR, Science and Engineering Research Board (SERB) [Research grant: SB/S1/OC-47/2103] and the Department of Science and Technology (DST), Government of India for financial support.

Author Contributions

K.R. and T.G. designed the project. N.N synthesised the probe, K.R. undertook the photophysical studies and *in vitro* studies of the probe, N.A.M., G.K. and H.M. Performed computational studies. All authors contributed to writing the manuscript.

Additional Information

Supplementary information accompanies this paper at http://www.nature.com/srep

Competing financial interests: The authors declare no competing financial interests.

How to cite this article: Rajasekhar, K. *et al.* A High Affinity Red Fluorescence and Colorimetric Probe for Amyloid β Aggregates. *Sci. Rep.* **6**, 23668; doi: 10.1038/srep23668 (2016).